Boosting Electrocatalytic Durability and Full Water Splitting Efficiency of $CoMoO_4$ via Strategic CeO_2 decoration

Tengfei Li,Zhirong Cao,Xiangdong Meng,Min Zhou , Yuxue Zhou*

College of Physical Science and Technology,Yangzhou University, Yangzhou 225002, China.

E-mail: yxzhou@yzu.edu.cn.

Details of iR Compensation Procedure

The uncompensated resistance (R_u) was measured by electrochemical impedance spectroscopy (EIS) at open circuit potential over a frequency range of 100 kHz to 0.1 Hz with an AC amplitude of 10 mV. The R_u value was obtained from the high-frequency intercept of the Nyquist plot with the real axis. To avoid risks associated with 100% real-time compensation, 90% automatic iR compensation was applied during all measurements.

For the CoMoO4/CeO2-CP-0.5 electrode (1 cm^2), the measured R_u was approximately 2.5 Ω. Based on Ohm's law, the total ohmic drop at 10 mA cm^{-2} is 25 mV, and the 90% compensation corresponds to a correction of 22.5 mV. This theoretical value is in excellent agreement with the observed 22 mV shift between raw and compensated curves , confirming the accuracy of the compensation and ruling out over-compensation.

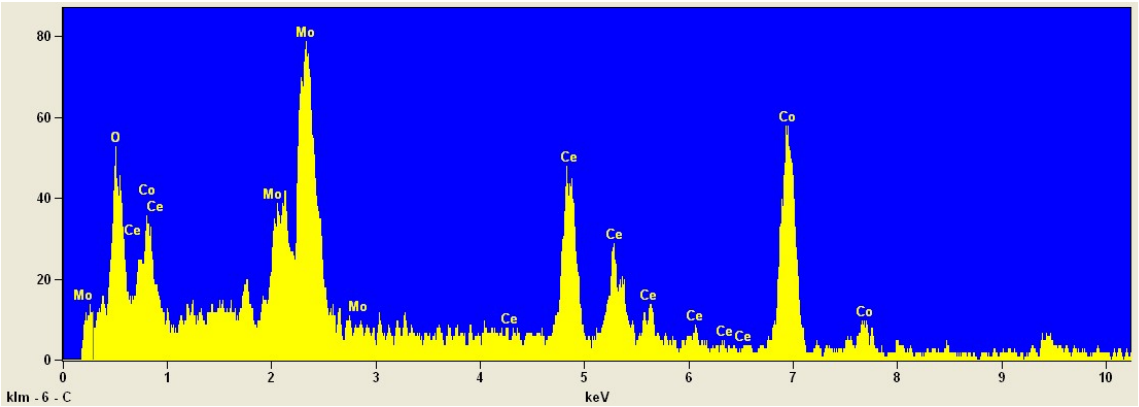

Fig. S1. EDX spectra of $CoMoO_4/CeO_2$-CP-0.5 sample.

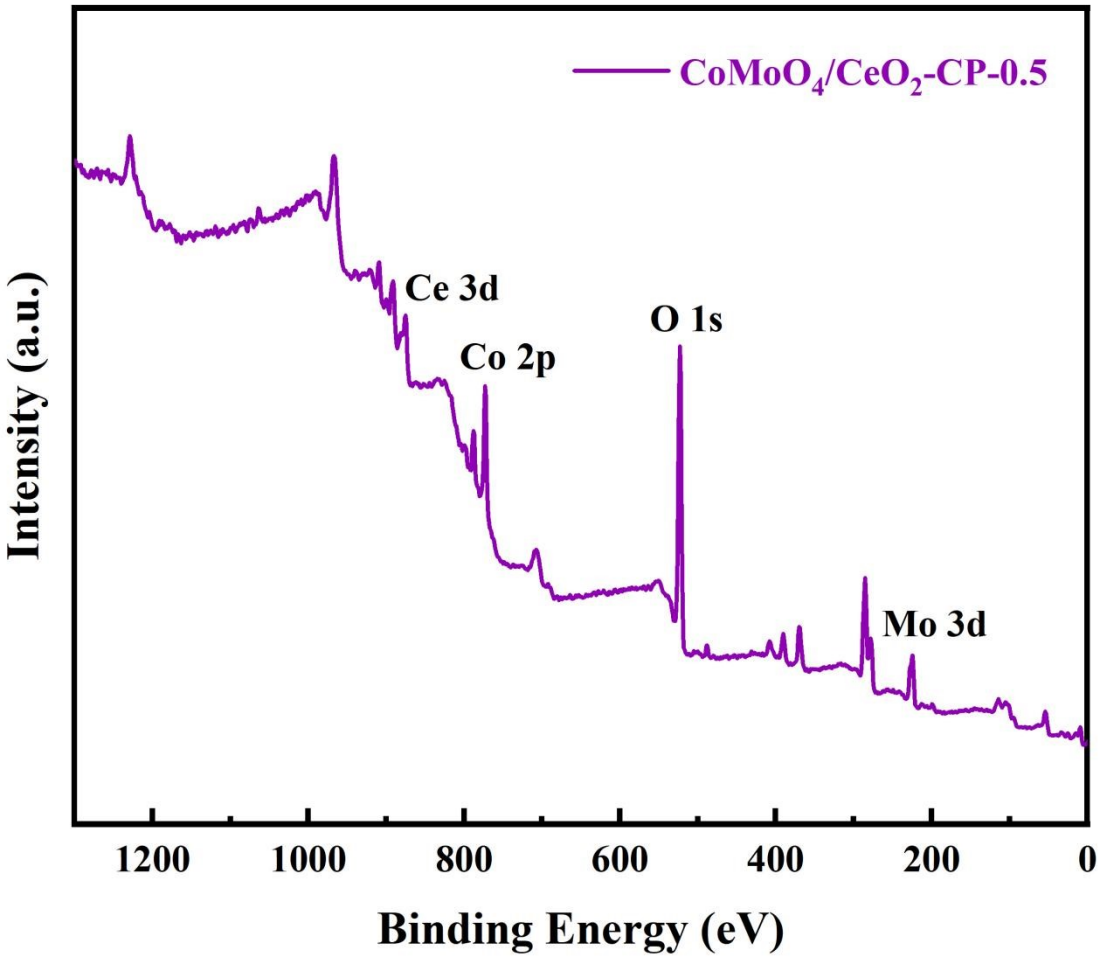

Fig. S2. XPS spectra of $CoMoO_4/CeO_2$-CP-0.5 catalyst.

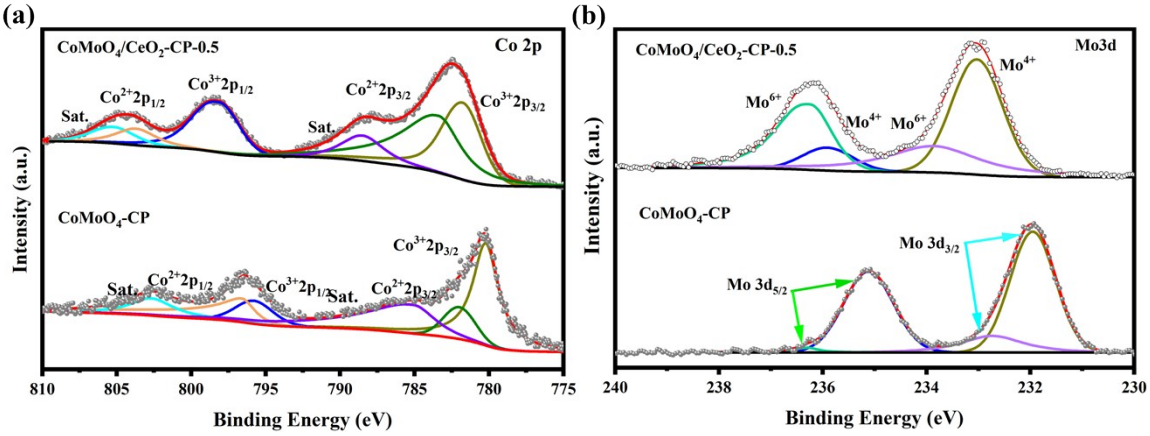

Fig. S3. (a) Co 2p XPS spectra for $CoMoO_4/CeO_2$-CP-0.5 and $CoMoO_4$-CP; (b)Mo 3d XPS spectra for $CoMoO_4/CeO_2$-CP-0.5 and $CoMoO_4$-CP.

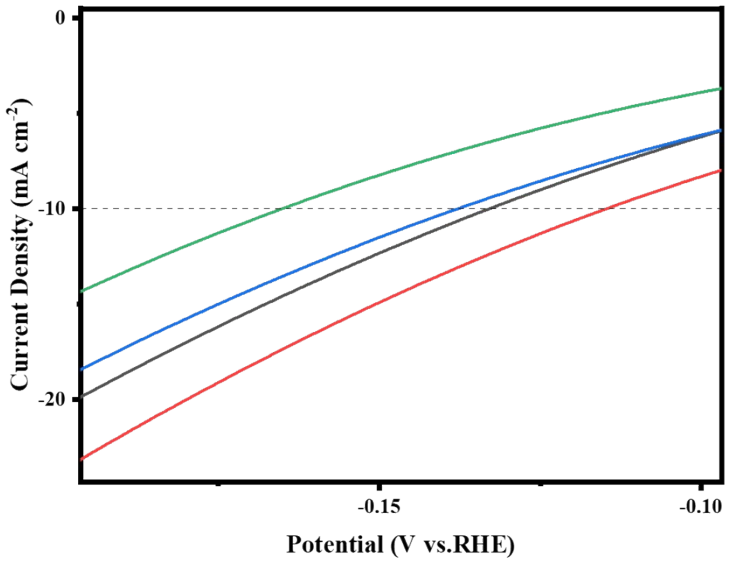

Fig. S4. HER activities of $CoMoO_4$-CP,$CoMoO_4/CeO_2$-CP-0.5,$CoMoO_4/CeO_2$-CP-0.6 and $CoMoO_4/CeO_2$-CP-0.8 in 1.0 M KOH: LSV plots(Partial enlarged view)

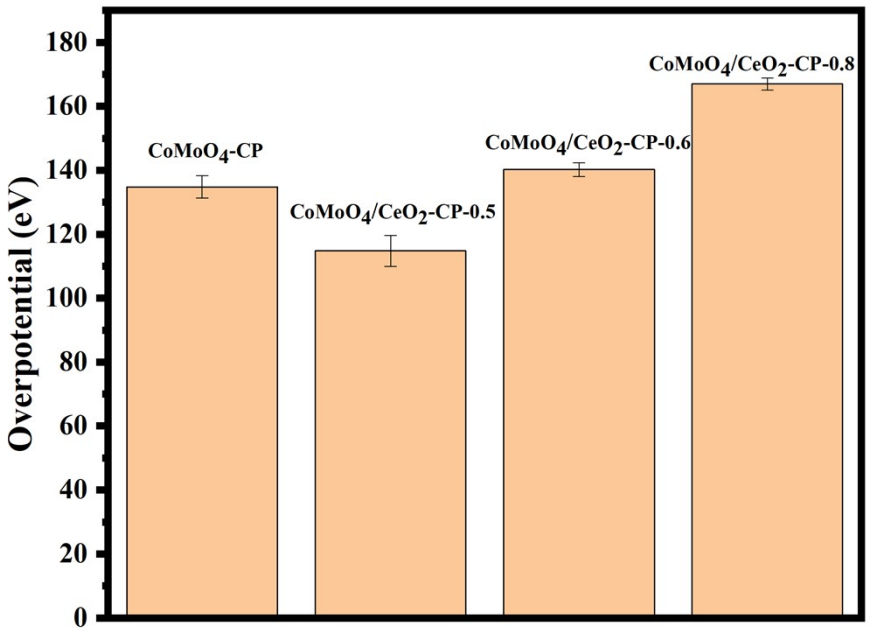

Fig. S5. Overpotentials at 10 mA cm^{-2} for HER with error bars from triplicate measurements from $CoMoO_4$-CP, $CoMoO_4/CeO_2$-CP-0.5, $CoMoO_4/CeO_2$-CP-0.6 and $CoMoO_4/CeO_2$-CP-0.8 in 1.0 M KOH,respectively.

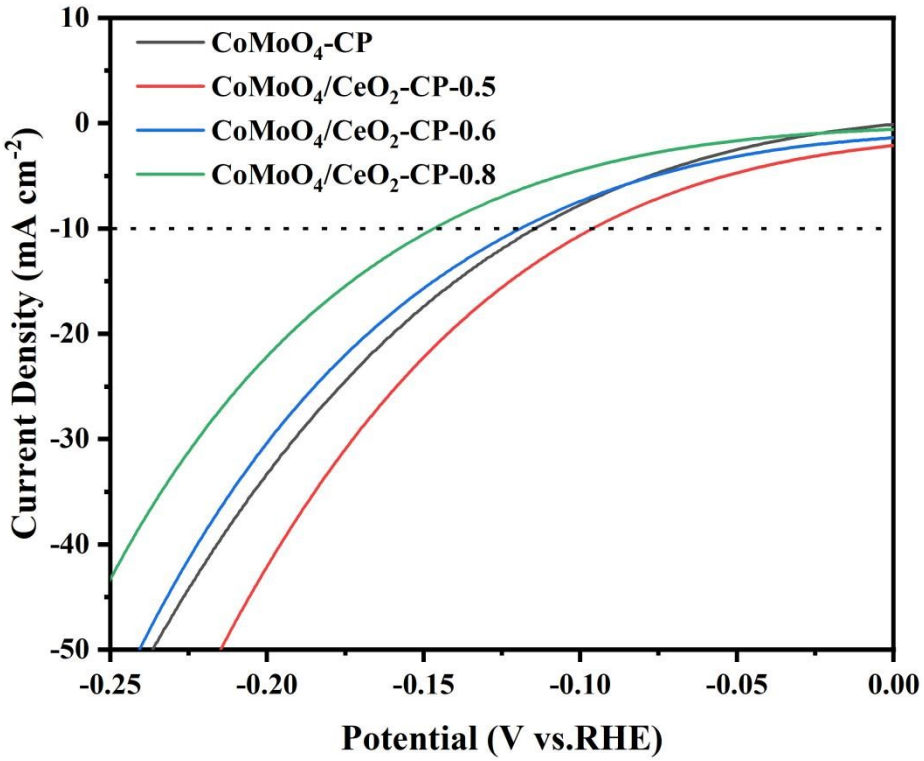

Fig. S6. iR-compensated HER polarization curves of $CoMoO_4$,$CoMoO_4/CeO_2$-CP-0.5, $CoMoO_4/CeO_2$-CP-0.6 and $CoMoO_4/CeO_2$-CP-0.8,respectively.

Table S1 Comparison of the HER performance of $CoMoO_4/CeO_2$-CP-0.5 at room temperature with other reported CeO_2-decorated electrocatalysts.

Catalyst	Overpotential（mV@ mA/cm²）	Reference
$CoMoO_4/CeO_2$-CP-0.5	114	This work
Mn–O–Ce/NiP	120	[1]
CeO_2/CuO	245	[2]
$CeO_2/CuO/Co_3O_4$	110	[3]
$CeO_2–Y_2O_3–Nd_2O_3$	303	[4]
CeO_2 -CoP/NF	124	[5]
$Ni(OH)_2$-CeO_2	207	[6]
CeO_2@$CoSe_2$/CC	138	[11]

Table S2 Fitting parameters of EIS for different electrodes(HER).

Catalyst	R_s (Ω)	R_{ct}(Ω)	CPE-T(Fcm^{-2})	CPE-P
$CoMoO_4$-CP	2.115	8.533	0.027	0.792
$CoMoO_4/CeO_2$-CP-0.5	2.529	5.637	0.047	0.874
$CoMoO_4/CeO_2$-CP-0.6	2.060	6.327	0.024	0.779
$CoMoO_4/CeO_2$-CP-0.8	2.067	6.247	0.029	0.781

Table S3 Fitting parameters of EIS for different electrodes(OER).

Catalyst	R_s (Ω)	R_{ct}(Ω)	CPE-T(Fcm^{-2})	CPE-P
$CoMoO_4$-CP	2.109	1.874	0.191	0.826
$CoMoO_4/CeO_2$-CP-0.5	2.493	1.550	0.069	0.892
$CoMoO_4/CeO_2$-CP-0.6	2.102	1.520	0.284	0.812
$CoMoO_4/CeO_2$-CP-0.8	2.065	1.784	0.162	0.849

Table S4 Comparison of the OER performance of $CoMoO_4/CeO_2$-CP-0.5 at room temperature with other reported CeO_2-decorated electrocatalysts

Catalyst	Overpotential（mV@ mA/cm^2）	Reference
$CoMoO_4/CeO_2$-CP-0.5	305	This work
CeO_2/CuO	410	[2]
$CeO_2/CuO/Co_3O_4$	520	[3]
RuO_2/CeO_2	350	[7]
Ag-CeO_2-Co_3O_4/C	340	[8]
Ni/CeO_2	335	[9]
NiS_x/CeO_2/NF	326	[10]

Ni-Co-CeO_2/Ni	301	[12]

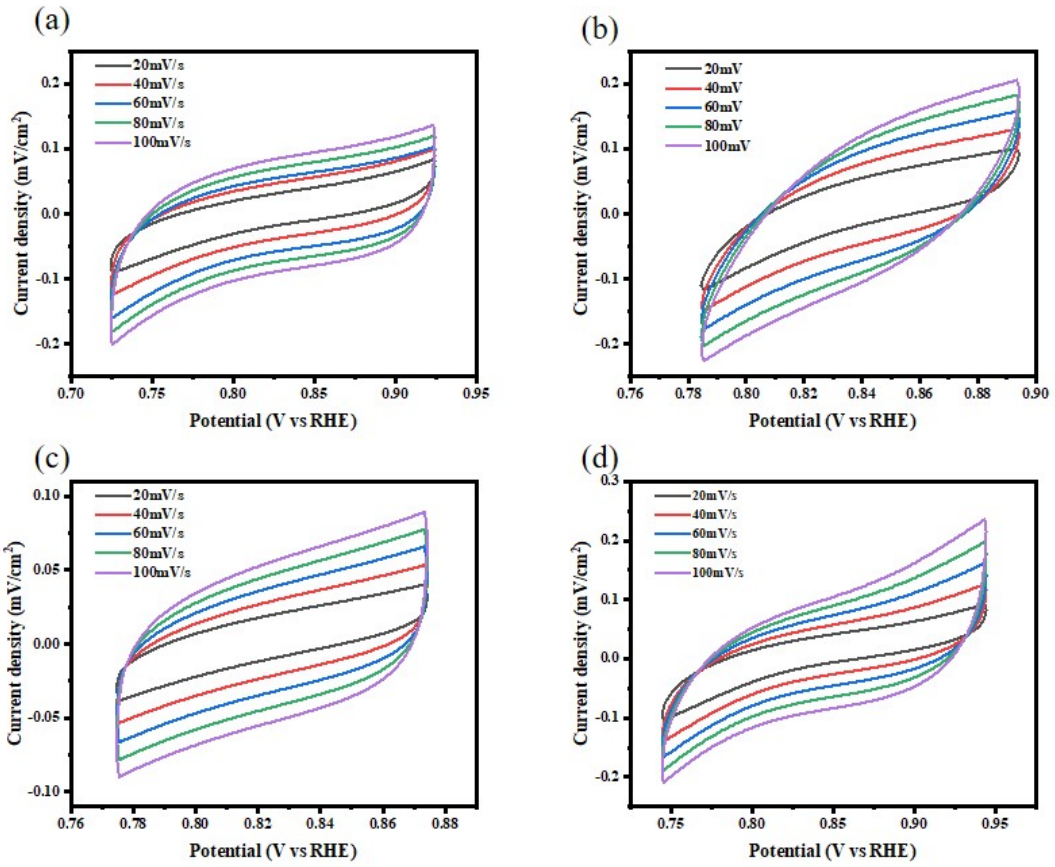

Fig.S7. HER activities: The cyclic voltammetry (CV) curves of (a) $CoMoO_4$-CP, (b) $CoMoO_4/CeO_2$-CP-0.5 , (c) $CoMoO_4/CeO_2$-CP-0.6, (d) $CoMoO_4/CeO_2$-CP-0.8 at various scan rates for the calculation of electrochemical double-layer capacitances.

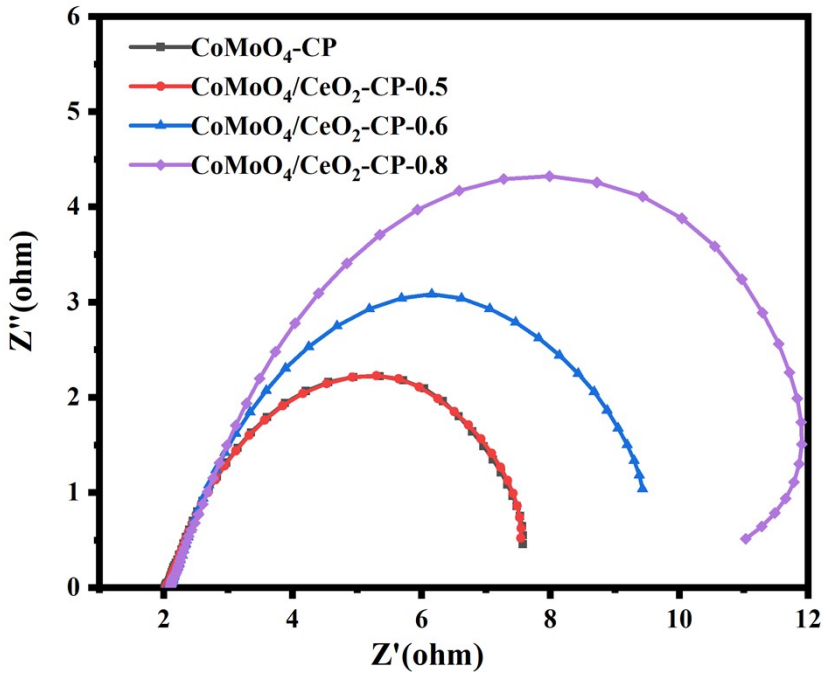

Fig. S8.EIS raw data from $CoMoO_4$-CP,$CoMoO_4/CeO_2$-CP-0.5,$CoMoO_4/CeO_2$-CP-0.6 and $CoMoO_4/CeO_2$-CP-0.8, respectively(HER).

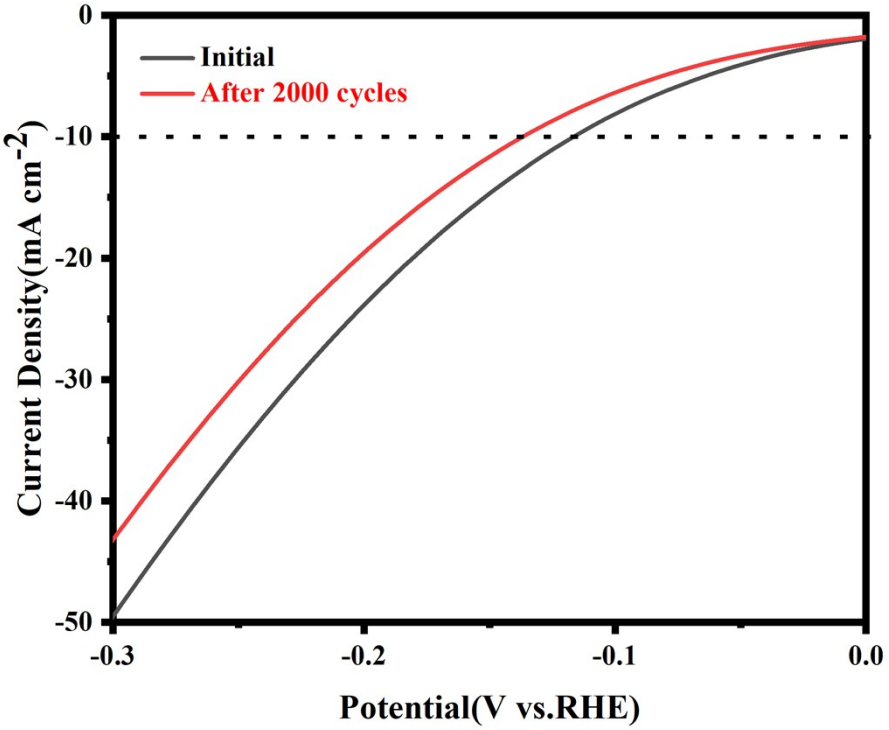

Fig. S9. Chronopotentiometric measurement of $CoMoO_4/CeO_2$-CP-0.5.

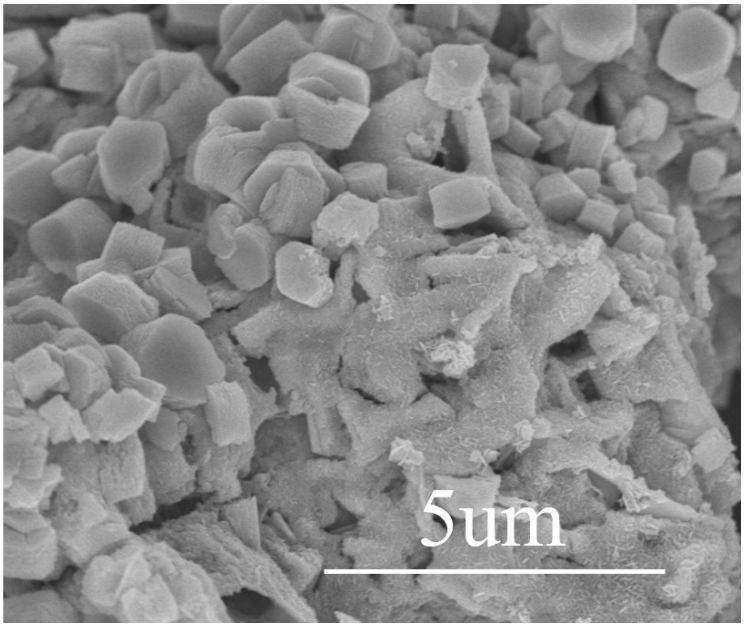

Fig. S10. SEM image of the $CoMoO_4/CeO_2$-CP-0.5 catalyst after long-term HER reaction

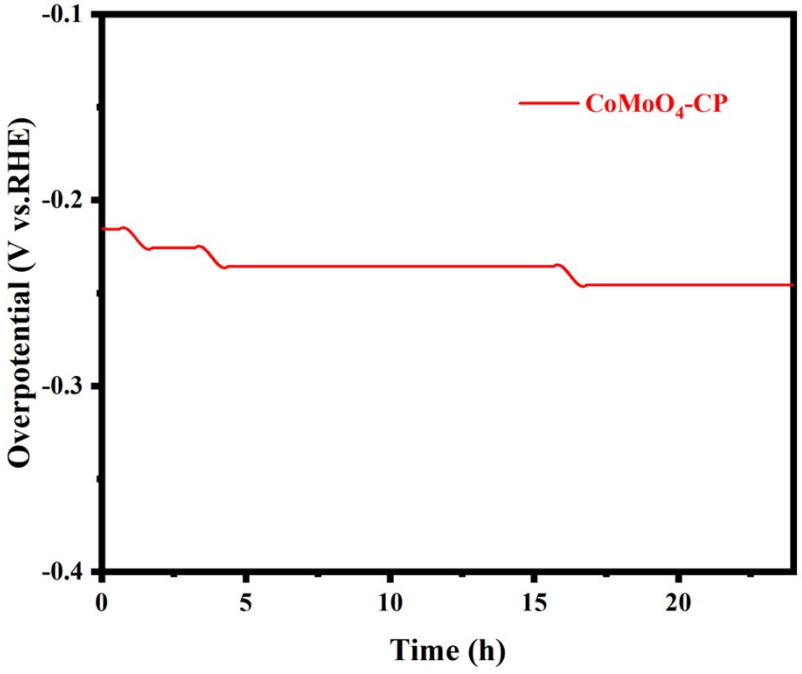

Fig. S11. Chronopotentiometric measurement of $CoMoO_4$-CP.

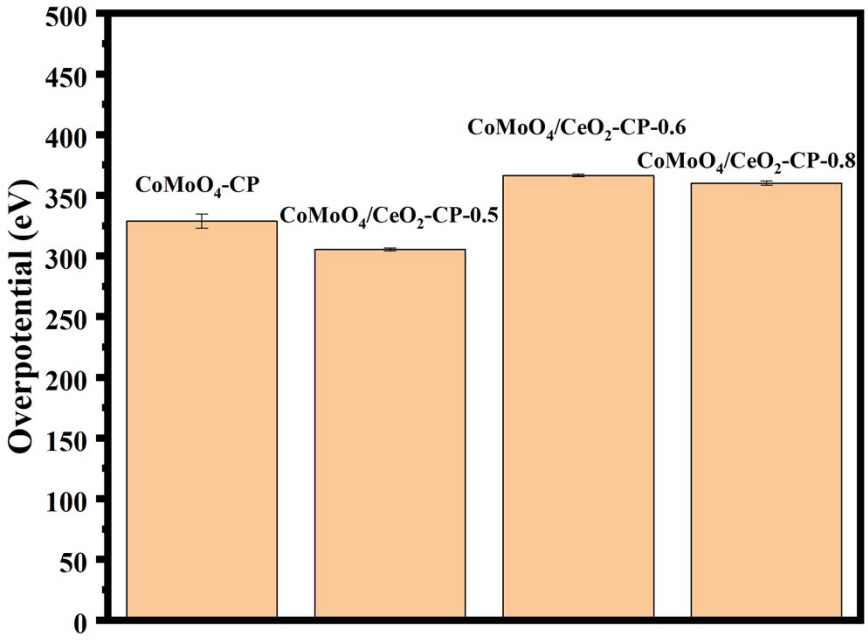

Fig. S12. Overpotentials at 10 mA cm^{-2} for OER with error bars from triplicate measurements from $CoMoO_4$-CP,$CoMoO_4/CeO_2$-CP-0.5,$CoMoO_4/CeO_2$-CP-0.6 and $CoMoO_4/CeO_2$-CP-0.8 in 1.0 M KOH,respectively.

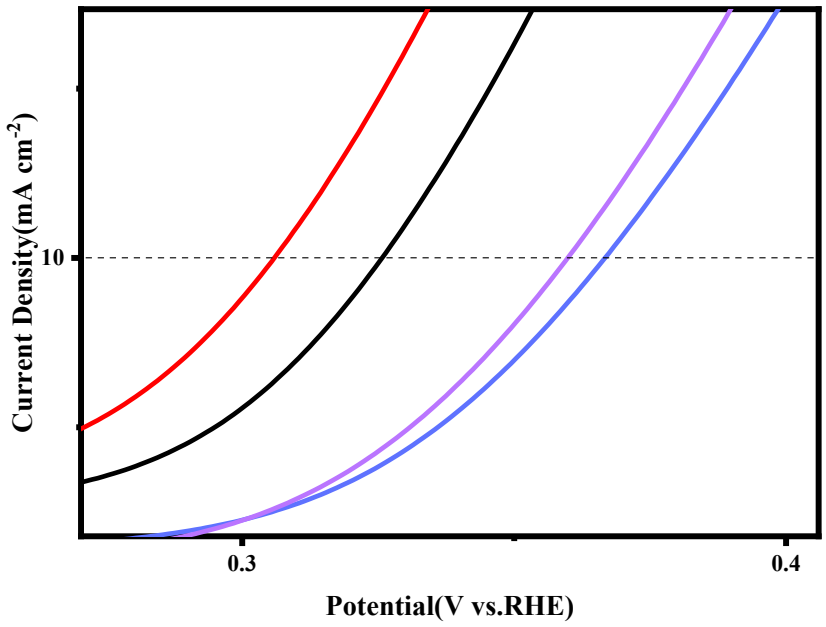

Fig. S13. OER activities of $CoMoO_4$-CP,$CoMoO_4/CeO_2$-CP-0.5,$CoMoO_4/CeO_2$-CP-0.6 and $CoMoO_4/CeO_2$-CP-0.8 in 1.0 M KOH: LSV plots(Partial enlarged view)

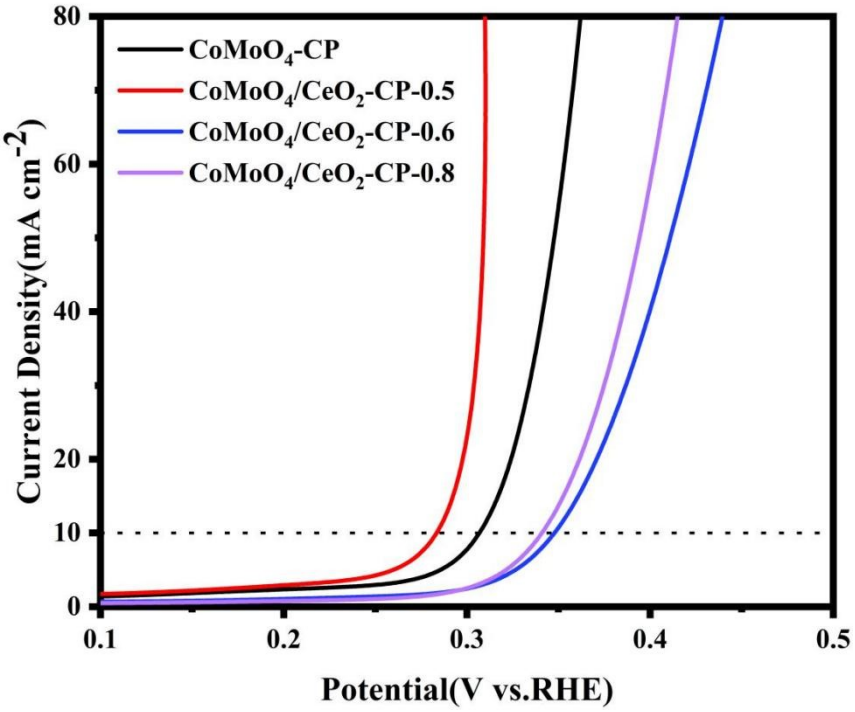

Fig. S14. iR-compensated OER polarization curves $CoMoO_4$,$CoMoO_4/CeO_2$-CP-0.5, $CoMoO_4/CeO_2$-CP-0.6 and $CoMoO_4/CeO_2$-CP-0.8,respectively.

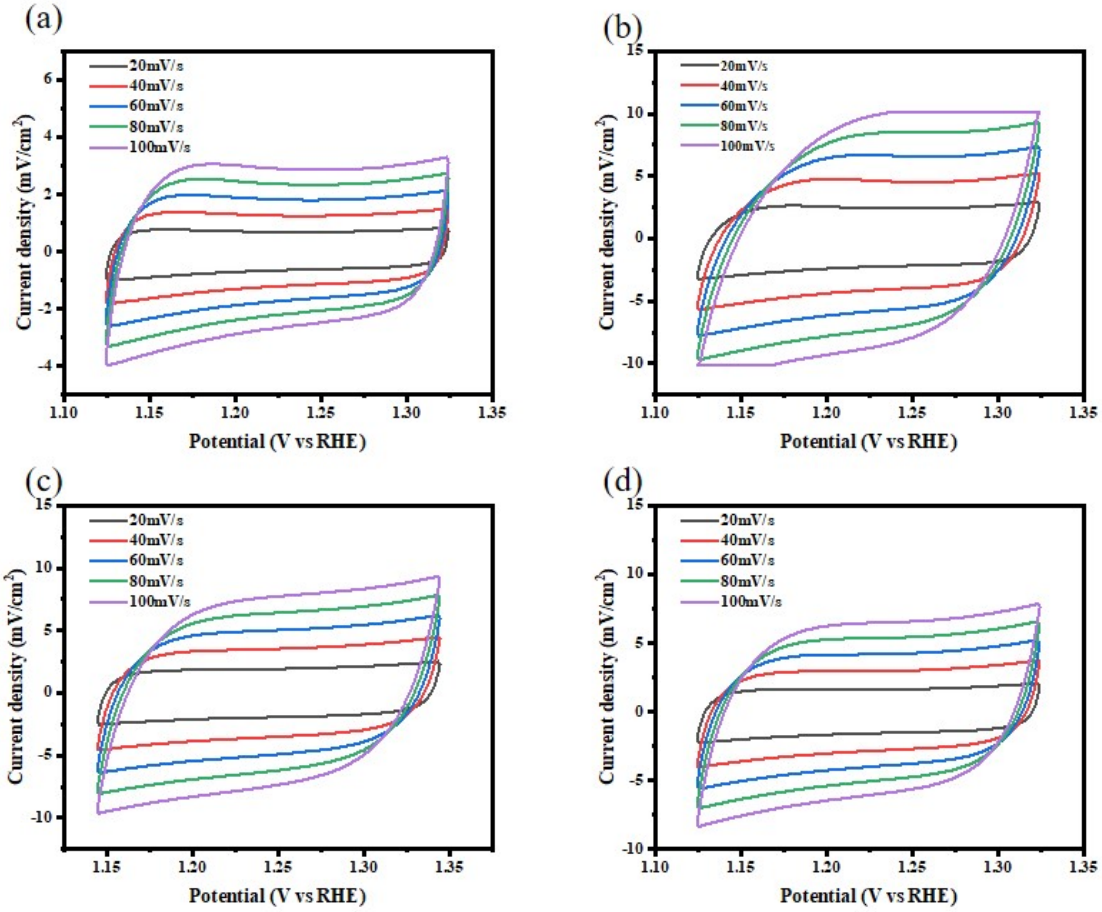

Fig.S15. OER activities: The cyclic voltammetry (CV) curves of (a) $CoMoO_4$-CP, (b) $CoMoO_4/CeO_2$-CP-0.5,(c)$CoMoO_4/CeO_2$-CP-0.6,(d) $CoMoO_4/CeO_2$-CP-0.8 at various scan rates for the calculation of electrochemical double-layer capacitances.

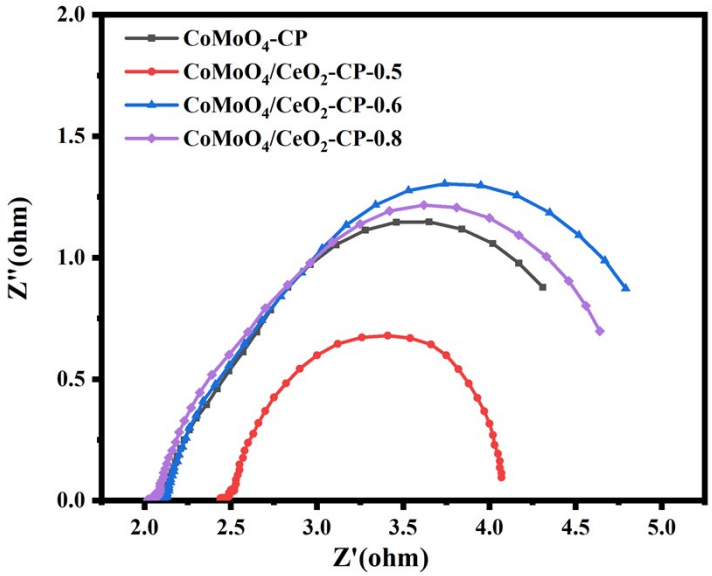

Figure S16. EIS raw data from $CoMoO_4$-CP,$CoMoO_4/CeO_2$-CP-0.5,$CoMoO_4/CeO_2$-CP-0.6 and $CoMoO_4/CeO_2$-CP-0.8, respectively(OER).

[1]. Remadevi T, Rajan A, Muhammed A, et al. Mn–Ce modified NiP electrocatalysts for HER: A combined computational and electrochemical study[J]. International Journal of Hydrogen Energy, 2025, 148: 150068.

[2]. Ghosh D, Pradhan D. Effect of cooperative redox property and oxygen vacancies on bifunctional OER and HER activities of solvothermally synthesized CeO_2/CuO composites[J]. Langmuir, 2023, 39(9): 3358-3370.

[3]. Shaghaghi Z, Jafari S, Mohammad-Rezaei R. The heterostructure of ceria and hybrid transition metal oxides with high electrocatalytic performance for water splitting and enzyme-free glucose detection[J]. Journal of Electroanalytical Chemistry, 2022, 915: 116369.

[4]. Shaghaghi Z, Jafari S, Mohammad-Rezaei R. The heterostructure of ceria and hybrid transition metal oxides with high electrocatalytic performance for water splitting and enzyme-free glucose detection[J]. Journal of Electroanalytical Chemistry, 2022, 915: 116369.

[5]. Qiu W J, Hu Z, Zhou Q H, et al. Rare earth cerium oxide reinforced cobalt based catalysts for electrolysed water and their properties[J]. Acta Materiae Compositae Sinica, 2024, 41: 804.

[6]. Xiang D, Qin Z, Gan Y, et al. Interfacial charge density modulation by coupling CeO_2 with dual-phase NiS/Ni_3S_2 to accelerate alkaline water splitting[J]. Materials Today Chemistry, 2023, 34: 101791.

[7]. Galani S M, Mondal A, Srivastava D N, et al. Development of RuO_2/CeO_2 heterostructure as an efficient OER electrocatalyst for alkaline water splitting[J]. International Journal of Hydrogen Energy, 2020, 45(37): 18635-18644.

[8]. Li T, He Z, Liu X, et al. Interface interaction of Ag-CeO_2-Co_3O_4 facilitate ORR/OER activity for Zn-air battery[J]. Surfaces and Interfaces, 2022, 33: 102270.

[9]. Gunarasan J P C, Lee J W. Superaerophobic 0D nickel–2D ceria supported 316L for enhanced OER and HER activity[J]. Surface and Coatings Technology, 2025, 507: 132143.

[10]. Zhang X, Liu F, Ji X, et al. Facile generation of CeO_2 nanoparticles on multiphased NiSx nanoplatelet arrays as a free-standing electrode for efficient overall water splitting[J]. Journal of Colloid and Interface Science, 2024, 653: 308-315.

[11]. Guo Q, Li Y, Xu Z, et al. CeO_2-accelerated surface reconstruction of $CoSe_2$ nanoneedle forms active CeO_2@ CoOOH interface to boost oxygen evolution reaction for water splitting[J]. Advanced Energy Materials, 2025, 15(4): 2403744.

[12]. Jiang W, Li H, Chen Y, et al. OER properties of Ni–Co–CeO_2/Ni composite electrode prepared by magnetically induced jet electrodeposition[J]. International Journal of Hydrogen Energy, 2023, 48(11): 4287-4299.